

# UC Irvine

## UC Irvine Previously Published Works

### Title

Growth Assessment of Native Tree Species from the Southwestern Brazilian Amazonia by Post-AD 1950 14C Analysis: Implications for Tropical Dendroclimatology Studies and Atmospheric 14C Reconstructions

### Permalink

<https://escholarship.org/uc/item/4bz9p8cr>

### Journal

Forests, 12(9)

### ISSN

1999-4907

### Authors

Santos, Guaciara M  
Rodriguez, Daigard Ricardo Ortega  
Barreto, Nathan de Oliveira  
et al.

### Publication Date

2021-08-31





### DOI

10.3390/f12091177

Peer reviewed

## Article

# Growth Assessment of Native Tree Species from the Southwestern Brazilian Amazonia by Post-AD 1950 <sup>14</sup>C Analysis: Implications for Tropical Dendroclimatology Studies and Atmospheric <sup>14</sup>C Reconstructions

Guaciara M. Santos <sup>1,\*</sup>, Daigard Ricardo Ortega Rodriguez <sup>2,\*</sup> , Nathan de Oliveira Barreto <sup>2</sup> , Gabriel Assis-Pereira <sup>2</sup>, Ana Carolina Barbosa <sup>3</sup>, Fidel A. Roig <sup>4,5</sup>  and Mário Tomazello-Filho <sup>2</sup> 

- <sup>1</sup> Earth System Science Department, University of California, B321 Croul Hall, Irvine, CA 92697-3100, USA
- <sup>2</sup> Departamento de Ciências Florestais, Escola Superior de Agricultura “Luiz de Queiroz”, Universidade de São Paulo, Piracicaba 13418-900, Brazil; nathan.barreto@usp.br (N.d.O.B.); gabriel\_assispereira@hotmail.com (G.A.-P.); mtomazel@usp.br (M.T.-F.)
- <sup>3</sup> Departamento de Ciências Florestais, Universidade Federal de Lavras, CP 3037, Lavras 37200-900, Brazil; anabarbosa@ufla.br
- <sup>4</sup> Argentine Institute of Nivology, Glaciology and Environmental Sciences (IANIGLA), CONICET-Universidad Nacional de Cuyo, Mendoza 5500, Argentina; froig@mendoza-conicet.gob.ar
- <sup>5</sup> Hémera Centro de Observación de la Tierra, Escuela de Ingeniería Forestal, Facultad de Ciencias, Universidad Mayor, Santiago 8580745, Chile
- \* Correspondence: gdossant@uci.edu (G.M.S.); dai.ricardo.or@usp.br (D.R.O.R.); Tel.: +1-(949)-824-98-51 (G.M.S.)



**Citation:** Santos, G.M.; Rodriguez, D.R.O.; Barreto, N.d.O.; Assis-Pereira, G.; Barbosa, A.C.; Roig, F.A.; Tomazello-Filho, M. Growth Assessment of Native Tree Species from the Southwestern Brazilian Amazonia by Post-AD 1950 <sup>14</sup>C Analysis: Implications for Tropical Dendroclimatology Studies and Atmospheric <sup>14</sup>C Reconstructions. *Forests* **2021**, *12*, 1177. <https://doi.org/10.3390/f12091177>

Academic Editor: Joana Vieira

Received: 6 August 2021

Accepted: 27 August 2021

Published: 31 August 2021

**Publisher’s Note:** MDPI stays neutral with regard to jurisdictional claims in published maps and institutional affiliations.



**Copyright:** © 2021 by the authors. Licensee MDPI, Basel, Switzerland. This article is an open access article distributed under the terms and conditions of the Creative Commons Attribution (CC BY) license (<https://creativecommons.org/licenses/by/4.0/>).

**Abstract:** Tree-ring width chronologies of cedro (*Cedrela fissilis* Vell.) (1875 to 2018), jatobá (*Hymenaea courbaril* L.) (1840 to 2018) and roxinho *Peltogyne paniculata* Benth.) (1910 to 2018) were developed by dendrochronological techniques in the southern Amazon Basin. Acceptable statistics for the tree-ring chronologies were obtained, and annual calendar dates were assigned. Due to the lack of long-term chronologies for use in paleoclimate reconstructions in degraded forest areas, dendrochronological dating was validated by <sup>14</sup>C analysis. Tree-rings selected for analysis corresponded to 1957, 1958, 1962, 1963, 1965, 1971, and 1972. Those are critical calendar years in which atmospheric <sup>14</sup>C changes were the highest, and therefore their tree-ring cellulose extracts <sup>14</sup>C signatures when in alignment with existing post-AD 1950 atmospheric <sup>14</sup>C atmospheric curves would indicate annual periodicity. Throughout our correlated calendar years and post-AD 1950 <sup>14</sup>C signatures, we indicate that *H. courbaril* shows an erratic sequence of wood ages. The other two tree species, *C. fissilis* and *P. paniculata*, are annual in nature and can be used successfully as paleoclimate proxies. Moreover, due to the sampling site’s strategic location in relation to the Tropical Low-Pressure Belt over South America, these trees can be used to enhance the limited amount of observational data in Southern Hemisphere atmospheric <sup>14</sup>C calibration curves.

**Keywords:** radiocarbon (<sup>14</sup>C) dating; tree-ring analysis; tropical dendrochronology; Amazon basin; lower latitudes

## 1. Introduction

Tree rings are an important source of high-resolution data for the long-term assessment of events occurring prior to instrumental data that characterize climate variability [1,2], and can be applied to calibrating and simulating climate, ecological, and physiological forecasting of forest ecosystems [3–6]. Hence, it is paramount that tree growth increments be continuous and their pattern well known so that climate indicators can be properly derived [7–9]. Moreover, tree ring research is relevant to atmospheric radiocarbon (<sup>14</sup>C) reconstructions [10,11]. Calibration curves are needed for converting <sup>14</sup>C dates to cal-

endar ages [12,13], and for studying the global carbon cycle [14,15] and the effects of anthropogenic activities on the environment and the climate system [16].

The majority of tree-ring chronologies (see [17]) with reliable cross-dating control of radial growth have been from ecoregions with well-defined seasons: e.g., the extra-tropics [18]. In the tropics, recent efforts and important methodological advances [19] have made it possible to increase the number of chronologies [5,6]. However, challenges in finding native species that can be dated to their formative calendar year still persist. Tropical wood anatomical features are highly diverse, and it is often problematic to identify the distinctness and boundaries of tree rings [20–23]. Besides their complex macroscopic wood anatomy, tropical species frequently present so-called tree-ring anomalies, such as wedging rings or partially missing rings, as well as false, discontinuous, and double-growth rings [6,9], which can lead to dating errors. Moreover, strong precipitation seasonality can lead to intra-annual phenology responses in deciduous or semi-deciduous tree species, triggering biannual ring formation [24]. Thus, it is desirable to match tree-ring chronologies obtained from traditional dendrochronological techniques (regardless whether they are complete or ongoing) with post-AD 1950  $^{14}\text{C}$  ages [25]. This enables independent validation of tree-ring width chronologies, and ensures data quality and consistency, even before broad comparisons of various paleo proxies are conducted.

Post-AD 1950  $^{14}\text{C}$  analysis of selected single tree rings works as a corroboration method thanks to the multiple aboveground thermonuclear detonations that occurred during the 1950s and 1960s [26], which caused atmospheric  $^{14}\text{C}$  levels to nearly double in the troposphere [14]. This anthropogenic  $^{14}\text{C}$  spike, and its subsequent decline once the Limited Test Ban Treaty was signed, allowed researchers to use the bomb  $^{14}\text{C}$  as an independent marker. Worldwide atmospheric  $^{14}\text{C}$  observations at sites in both the Northern and Southern Hemispheres have been used to establish atmospheric  $^{14}\text{C}$  calibration curves across the globe [27]. In the Neotropical realm, direct comparisons of  $^{14}\text{C}$  content in cellulose fibers extracted from a tree-ring wood sample of known age have helped confirm tree species growth patterns as annual [10,11,28–31], problematic [21], or occurring twice a year [24]. This method has also helped scientists to identify consistent wood layers corresponding to seasonal or annual growing periods in tree species at several other major ecological regions, such as Mediterranean climatic areas [20,31], subtropical rainforest [22], and tropical savanna [32], for example.

Tree-ring width chronologies were developed for the first time for tree species of cedro (*Cedrela fissilis* Vell.) (1875 to 2018), jatoba (*Hymenaea courbaril* L.) (1840 to 2018), and roxinho (*Peltogyne paniculata* Benth.) (1910 to 2018) from the Jamari National Forest (JNF), state of Rondônia, located in the southwestern Brazilian Amazon (Figure 1). The synchronism of ring width patterns among radii and individuals was determined by visual and statistical comparisons, applying standard dendrochronological methods. Two of the three species studied here, *C. fissilis* [33–35] and *H. courbaril* [28,36,37], have been studied previously elsewhere, via methods of cambial wounding, cross-dating, and/or  $^{14}\text{C}$  dating, and were characterized as annual in nature. On the other hand, the genus *Peltogyne* has barely been studied (i.e., [25,38]) and *P. paniculata* chronology has not yet been reported. Therefore, this work represents the first ring-width chronology assessment and  $^{14}\text{C}$  validation for this single tree species.

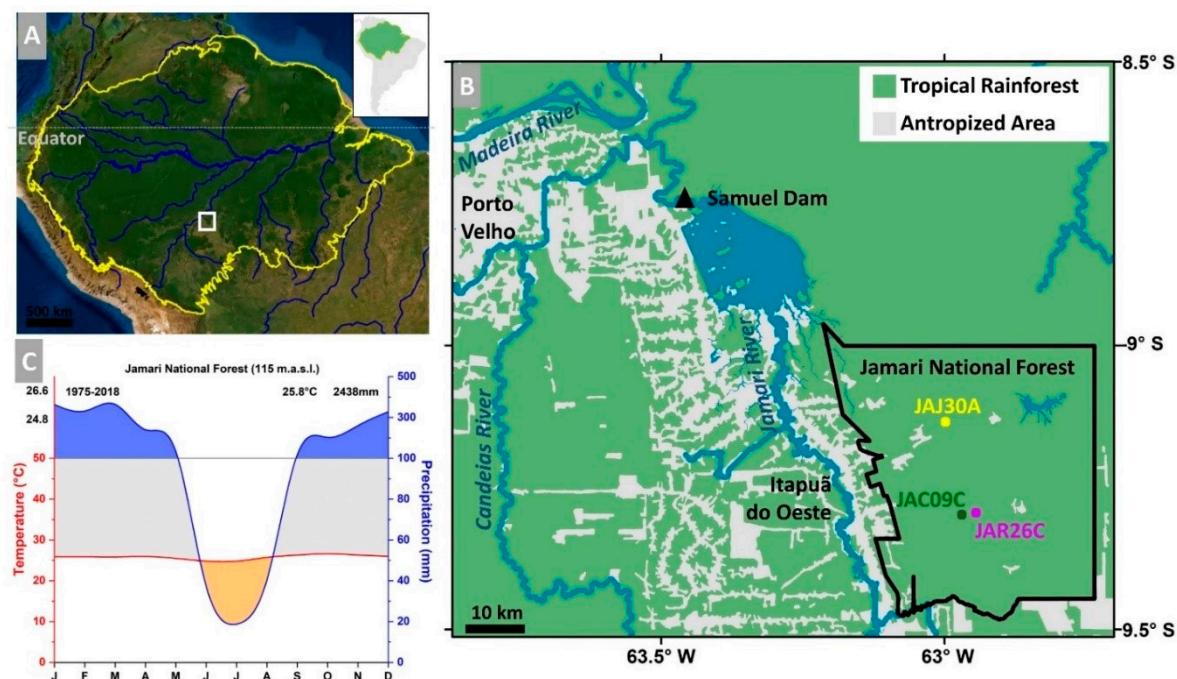


**Figure 1.** (A) Map of the study area in the southern Amazon Basin-cutting block (white) illustrates the location of JNF. (B) Close view of JNF with its boundary clearly demarcated as well as the specific sites of the three tree species collected for  $^{14}\text{C}$  dating: i.e., JAC09C: *Cedrela fissilis*, JAJ30A: *Hymenaea courbaril*, and JAR26C: *Peltogyne paniculata*. Other features are main rivers, location of the dam across the Jamari River, and closest cities. (C) Climate diagram of Walter and Lieth, based on regional meteorological and hydrological records from 1975 to 2018 (data collected from HIDROWEB v3.1.1, Agência Nacional das Águas, and Instituto Nacional de Pesquisas Espaciais—<http://bancodedados.cptec.inpe.br>, accessed on 18 April 2021), indicates that the dry season occurs from June to August. Solid blue areas show the months with rainfall above 100 mm. The values in black at the top right are the mean annual temperature and the total annual precipitation. Values in black on the left axis are the maximum and minimum annual temperatures. The altitude of the JNF is given in m above sea level (m.a.s.l.).

The southwestern Brazilian Amazon, and especially the state of Rondônia, has been facing substantial forest losses since the late 1980s due to intense human activities across its territory's land surface [39]. Our studied site is located at the heart of this accelerated land cover change area, which, after three decades of increased deforestation, fires, and forest fragmentation, has been experiencing dramatic changes in seasonal precipitation chemistry [40] and regional hydroclimate shifts [41,42], which can potentially impact the livelihoods of people in the state [43].

Therefore, the development of new reliable tree-ring chronologies can situate modern and future climate change in a long-term pre-industrial perspective. Moreover, the JNF's strategic location (9.3° S, 62.9° W) can provide key data related to the Tropical Low-Pressure Belt (TLPB, conventionally termed Inter-Tropical Convergence Zone) [44] and the South American Monsoon System [45], and enable exploration of the stability of ocean-atmospheric forcing of climate over Amazonia. Thus, given the urgent need to build reliable climate-sensitive century-long tree-ring chronologies across the Amazon basin [46,47] and the site's strategic location, these dendrochronologically dated tree species were independently evaluated by high-precision (<0.3%) post-AD 1950  $^{14}\text{C}$  accelerator mass spectrometer (AMS) analysis. Seven calendar years for each tree species were selected to undergo  $\alpha$ -cellulose extractions and subsequent sample processing for  $^{14}\text{C}$ -AMS measurements at the Keck Carbon Cycle Accelerator Mass Spectrometer (KCCAMS) at the University of California, Irvine (UCI). Dendrochronologically dated tree rings and their  $^{14}\text{C}$  values were then compared to the Southern Hemisphere (SH) atmospheric post-AD 1950  $^{14}\text{C}$  bomb curves (SH zone 1–2 & SH zone 3), using the current spatial distribution

of bomb-pulse  $^{14}\text{C}$  as defined in [27] and the independent dataset of Minas Gerais, Brazil (22° S; e.g., [10]).

## 2. Materials and Methods

### 2.1. Study Area

The study was conducted in the JNF (Figure 1), which comprises an area of 220,000 hectares located in the southern Amazon Basin between the geographic coordinates 09°00'00"–09°30'00" S and 62°44'05"–63°16'54" W [48]. The closest city is Itapuã do Oeste, with a population density of just 2.10 people per km<sup>2</sup> [49]. Based on monthly/seasonal maps and composite modeling [44], our studied data is believed to be located primarily within the “U-shape” of the TLPB that encompasses the Amazon Basin. As already mentioned, this region also is characterized by strong seasonal variability due to the South American Monsoon System, which represents one of the most prominent summertime climate patterns in South America [45].

This region’s native vegetation corresponds to the Open Ombrophilous Forest type, with a canopy height of around 20–25 m and emerging trees reaching 30–35 m, dominated by valuable timber species [40–52]. The annual average temperature in this region is 26 °C, and the average annual rainfall is 2438 mm, with well-defined dry and moderate water deficit conditions during the winter months of June and August (Figure 1C). The soil is classified as Yellow Dystrophic Latosol according to the Brazilian Soil Classification System [53].

### 2.2. Species Selection, Sample Collection, and Preparation

Three species were selected that had better characteristics for performing dendrochronological studies, as indicated in preliminary works: *Cedrela fissilis* Vell. (Meliaceae) [33,34], *Hymenaea courbaril* L. (Fabaceae) [36], and *Peltogyne paniculata* Benth (Fabaceae) [38].

All three species are deciduous [38,54–56], indicating that rainfall is probably the limiting factor promoting annual tree ring formation [57]. According to the literature, the growth period of *C. fissilis* [54], *H. courbaril* [58], and *Peltogyne* cf. *heterophylla* [25], a congeneric species of *P. paniculata*, should coincide with the rainy season, which generally falls between September (previous year) and the end of May (current year) (Figure 1C).

Samples were collected inside the Annual Production Unit (UPA in Portuguese, meaning the delimited area designated for forest management during the current year) in 2019 from the logging firms AMATA and MADEFLONA, both legal private companies operating the 96,000 ha of the JNF under sustainable management practices [48]. One disc from each of the 29 *C. fissilis*, 53 *H. courbaril*, and 40 *P. paniculata* trees was cut at the top level of the first log (6 m) of the felled trees (Figure 2A), following the methodology described in [47]. The samples were collected at log yards where recently cut logs (April to May of 2019) were stored. Three or four radial wood sections from each disc were cut and transported to the Wood Anatomy and Dendrochronology Laboratory from the ESALQ, University of São Paulo.

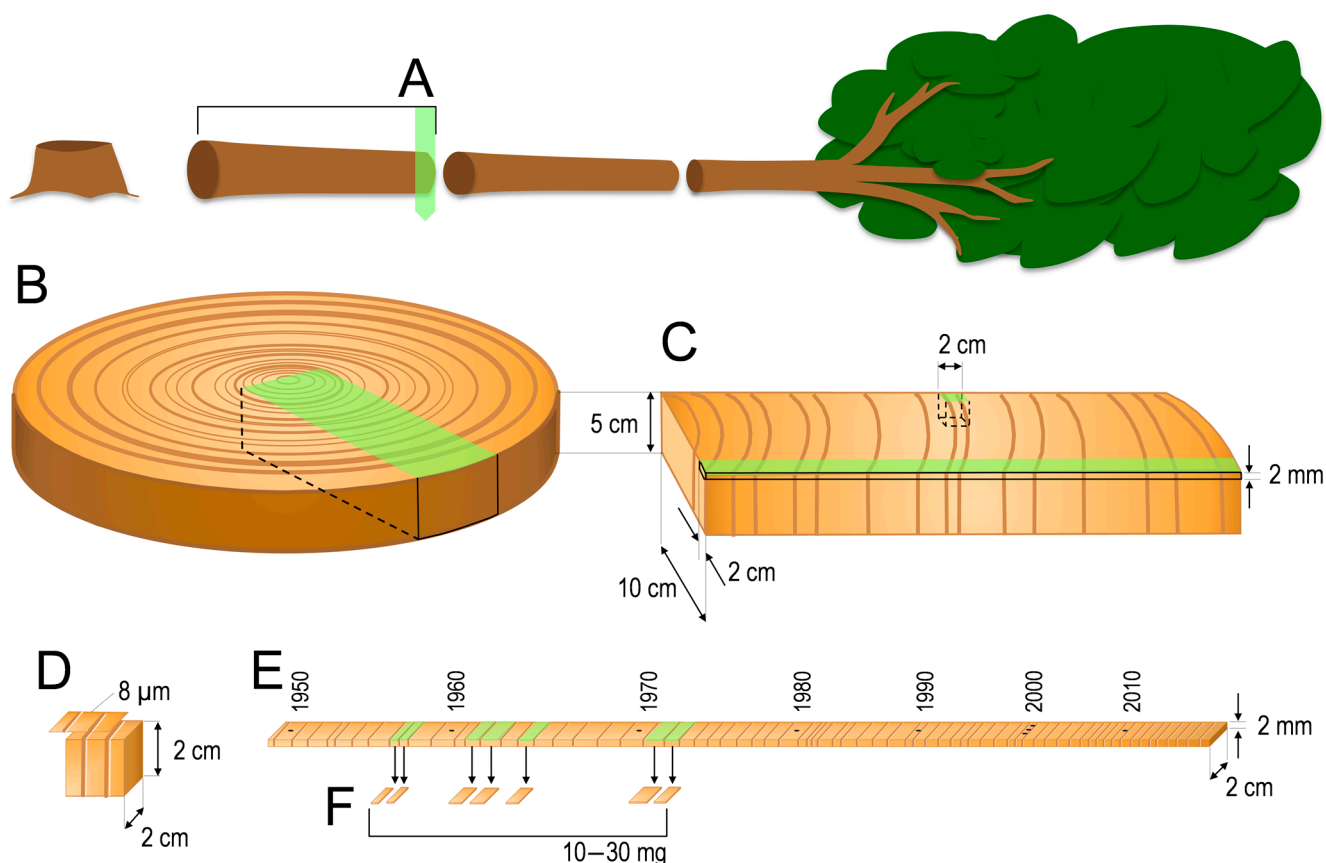


**Figure 2.** Scheme of preparation of wood samples for tree-ring analysis and  $^{14}\text{C}$  measurements. Cross sections were cut from the top of first log of recently felled trees (A); radial sections were cut from cross sections (B), polished and scanned (C); wood cube specimen (D) was cut for histological slides of transverse plane and microscopic analyses; a thin radial specimen was cut for X-ray densitometry analyses (E). After dating, wood material was collected for  $^{14}\text{C}$  measurements from each selected ring (calendar years: 1957, 1958, 1962, 1963, 1965, 1971 and 1972) by sampling the whole growing season between marginal parenchyma (F).

The transverse surfaces of the radial sections (10 cm width and 5 cm thickness) were polished with sandpaper (80–600 grit) to reveal the growth rings at the macroscopic level and scanned (1200 dpi resolution) to allow image analysis of the growth rings. To evaluate the microscopic anatomical tree-ring structure, a wooden cube specimen ( $2 \times 2 \times 2$  cm) was cut from each sample to obtain histological slides of the transverse plane (Figure 2D). A thin radial specimen (2 cm width and 2 mm thickness) was cut transversely, conditioned to 12% moisture [59], scanned in an X-ray densitometry chamber (Faxitron MX20-DC12, Faxitron X-ray, Lincolnshire, IL, USA), and the grayscale images analyzed to aid the tree-ring boundary delimitations (Figure 2E).

### 2.3. Tree-Ring Demarcation Strategies and Analysis

After transverse surface, histological, and X-ray grayscale images were collected, tree-ring structures were evaluated both macroscopically and microscopically to identify the wood anatomical markers for ring boundaries and measure ring widths (Figure 3). Tree-ring boundary delimitation was performed by combining wood anatomy techniques and X-ray densitometry analysis [59].

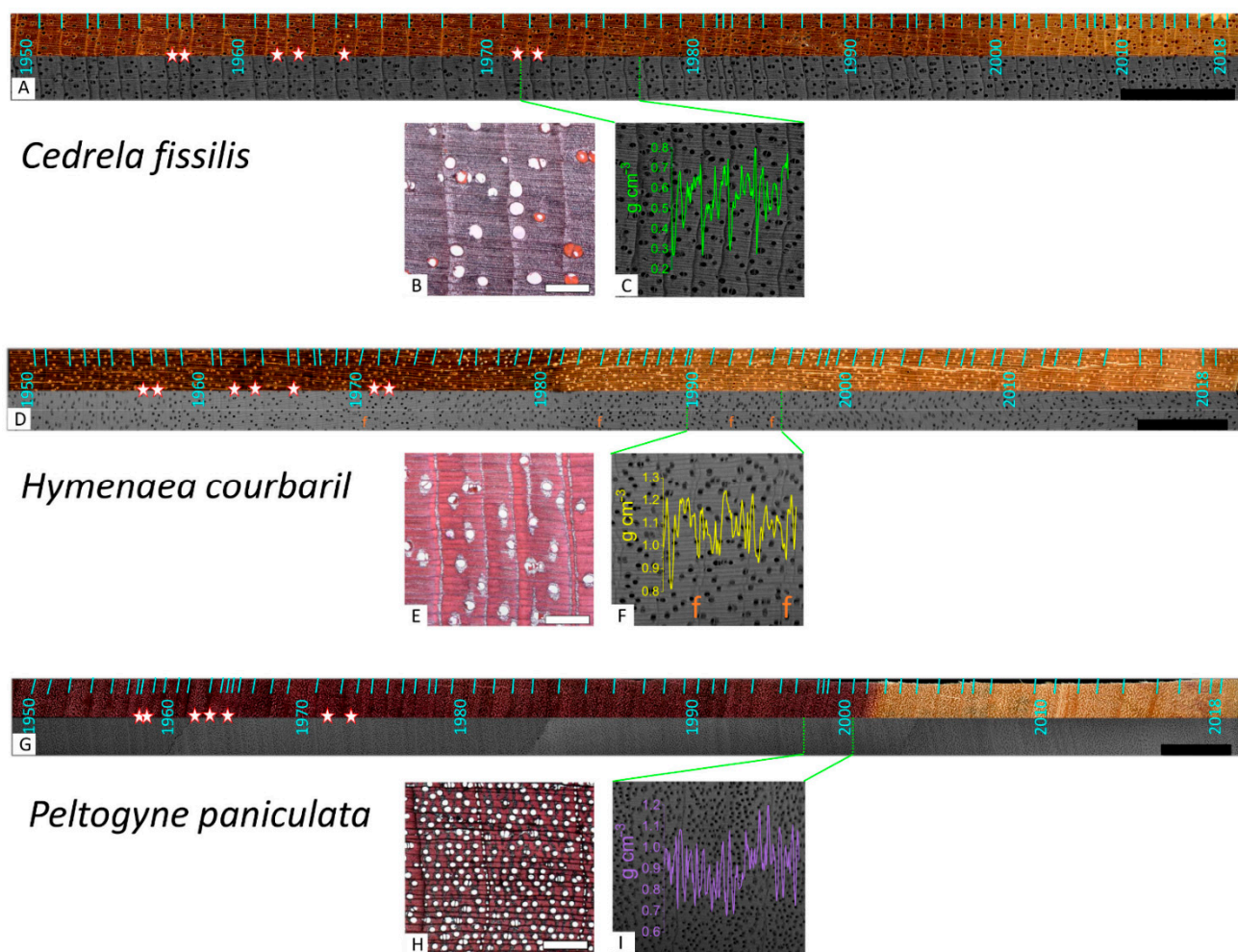


**Figure 3.** Transverse surfaces and grayscale images from X-ray of the radial sections (A,D,G, black bars = 10 mm) with growth ring boundaries delimited (light blue lines) and rings selected for  $^{14}\text{C}$  dating (white stars). The wood anatomy of the three species' tree-ring boundaries is formed by marginal parenchyma (B,E,H, white bars = 500  $\mu\text{m}$ ), associated with wood density values that decrease sharply at the end of the latewood (C,F,I). Orange "f" represents false *H. courbaril* rings detected by cross-dating.

Growth ring structures appear to be well-formed in the three studied species. Tree rings were cross-dated within (3–4 radii per tree) and among trees using skeleton plots, then dated and measured in CDendro and CooRecorder<sup>®</sup> software [60]. The dating accuracy was then checked with the computer program COFECHA [61]. Ring-width series were detrended and standardized using an age-dependent spline, and the robust mean index "standard" chronology was computed using the ARSTAN computer program [62,63]. Each species' standardized chronology was selected and characterized using the following statistical parameters: first-order autocorrelation, mean inter-correlation among all series (RBAR; e.g., [64]), and the expressed population signal (EPS; e.g., [65]).

#### 2.4. Radiocarbon Dating

Seven single rings from *C. fissilis*, *H. courbaril* and *P. paniculata* trees that were associated with the calendar years of 1957, 1958, 1962, 1963, 1965, 1971, and 1972 (Figure 3) were sampled for  $^{14}\text{C}$  analysis at the Wood Anatomy and Tree-ring Laboratory, ESALQ, University of São Paulo (LAIM/ESALQ/USP). These calendar years are from a period where the differences in atmospheric  $^{14}\text{C}$  between consecutive calendar years are the highest. Moreover, four of the individual tree rings selected represent calendar years from

the ascending portion of the atmospheric  $^{14}\text{C}$  bomb peak: one from the peak itself, and the remaining from the descending side of it. Wood material between 10 and 30 mg was collected from each selected ring (the whole growing season) by separating them at the marginal parenchyma, being careful not to include any material from neighboring rings (Figure 2E). Samples were then labeled by their core identifiers and calendar dates, packed, and shipped to KCCAMS/UCI for chemical extraction to  $\alpha$ -cellulose, graphite target processing, and  $^{14}\text{C}$  analysis. At KCCAMS/UCI,  $\alpha$ -cellulose was isolated following a method adapted from [66], with pre-baked 13 mm culture tubes used as chemical treatment vials. Wood aliquots were initially reduced to chips and re-weighed to check wood losses during cutting (<3%). Next, they were subjected to lignification and chlorification by means of an acid-base-acid pretreatment (1N HCl and NaOH at 70 °C for 30 min each, until supernatant was clear) [67], followed by a bleaching step (1N HCl and 1M NaClO<sub>2</sub> at 70 °C in a fume hood for approximately 6 h) to isolate holocellulose. Hemicellulose was then removed in a 17.5% NaOH solution at room temperature for approximately 1–2 hrs maximum, followed by one rinsed with 1N HCl to remove any labile atmospheric CO<sub>2</sub> uptake during the NaOH treatment [68]. The final insoluble organic portion is referred to as  $\alpha$ -cellulose, and it was subsequently rinsed with warm ultrapure water (~18 M $\Omega$ .cm) until pH 6 was reached, then homogenized, dried, and stored for later processing.

To produce solid graphite for  $^{14}\text{C}$ -AMS measurements, about 2 mg of  $\alpha$ -cellulose from each selected calendar year from the chronologies of JNF were loaded in pre-baked quartz tubes and evacuated-sealed to undergo combustion at 900 °C. We also chose to produce duplicates from either 1962 or 1963  $\alpha$ -cellulose extracts, depending on the amount of extracted material available from these calendar years in each chronology series. The measurement of wood material from these calendar years, which falls into the rising slope of the bomb-peak, potentially can be biased by small differences during the sampling of the rings (separation from cross-section and neighboring rings), reduction to chips before chemical treatment is applied (losses of wood during cutting), and/or poor homogenization of the final  $\alpha$ -cellulose fibers. Therefore, a high degree of agreement between duplicates would prove that our procedures are meaningful for this type of  $^{14}\text{C}$  investigation.

The CO<sub>2</sub> produced during combustion was cryogenically separated from other gasses and then reduced to filamentous graphite by Zn processing, following established protocols (e.g., [68], and references therein). Two wood reference materials, AVR wood-blank ( $^{14}\text{C}$ -free) and barley mash FIRI-J (post-AD 1950  $^{14}\text{C}$ ), were processed alongside samples to facilitate background corrections and quality control of the chemical extractions. Filamentous graphite was pressed into Al target holders and measured using an in-house modified 500 kV compact AMS unit (NEC 0.5 MV 1.5SDH-21 spectrometer from National Electrostatics Corporation, Middleton, WI) [69]. The samples'  $^{14}\text{C}/^{12}\text{C}$  ratios were normalized to six known standards of oxalic Acid I (OX-I; SRM4990B) from the National Institute of Standards and Technology (NIST, Gaithersburg, MD, USA). The emerging result was then corrected for isotopic fractionation by online- $\delta^{13}\text{C}$  measured directly loop-by-loop at the spectrometer, and background corrected by the  $^{14}\text{C}/^{12}\text{C}$  ratio of the  $\alpha$ -cellulose extracted wood blank [70]. A final value for the fraction of modern carbon ( $F^{14}\text{C}$ , defined as the ratio of the sample's radioactivity to the modern standard's radioactivity [71]) was reached using calculations from [72]. Graphite targets produced from combustible organics, such as POC coal from USGS, oxalic Acid II (OX-II) from NIST, and sucrose from ANU, were also analyzed for further quality assessment of the instrument. Overall, the measurements' precision and accuracy were better than 0.2%.

### 3. Results and Discussion

#### 3.1. Tree-Ring Demarcation

The conventional procedure used to determine the presence or absence of growth rings is to distinguish macroscopic anatomical patterns in the cross-section of the xylem [8,73]. In our study, these morphological changes were also verified by X-ray densitometry (Figure



3C,F,I). The potential of X-ray densitometry techniques to characterize and delimit tree rings has been increasingly validated for tropical species (e.g., [74–78]).

Similar to other tropical regions, in JNF the genera *Cedrela* [79], *Hymenaea* [80], and *Peltogyne* [81] presented well-defined growth rings useful for dendrochronological studies. The three genera present growth rings marked by marginal parenchyma. They were also characterized by a progressive increment of wood density values between the transition of early- and latewood, related to thick-walled fibre formation. Density values fall sharply at the end of the latewood. This density decrease observed in *C. fissilis* was related to the increase in the diameter and frequency of vessels and the initial-marginal parenchyma at the beginning of the earlywood (Figure 3B,C). In *H. courbaril*, it was related to the marginal parenchyma (Figure 3E,F), and in *P. paniculata*, it was related to the thin parenchyma band associated with the intercellular canals (Figure 3H,I). Both species showed a slight or no variation in vessel diameter and frequency between the early- and latewood transition.

The combined use of anatomical and X-ray densitometry techniques helped the observation and detection of the thin layer of marginal parenchyma cells in *P. paniculata* and *H. courbaril* by improving the observation of the marginal parenchyma bands, which, having few cells (Figure 3E,H), are difficult to observe in the dark purple heartwood of *P. paniculata* (Figure 3G) and in the clear cream sapwood of *H. courbaril* (Figure 3D). The intra- and interannual wood density profiles, as physical parameters of the wood provided by X-ray densitometry, are related to variations in the wood anatomy and can contribute to the definition of the ring boundaries [77,78].

### 3.2. Tree-Ring Chronologies

After identifying growth ring boundaries, the verification of the annual ring periodicity is a key point for the construction of chronologies [7–9]. The main strategy for performing this verification is the cross-dating between trees due to synchronized growth triggered by the annual climate cycle [57]. In the present study, the tree-ring width chronology of *C. fissilis* (1832 to 2018) based on 72 radii from 22 trees (76% of all sampled trees) presented a significant mean correlation among the series ( $r = 0.51$ ,  $p < 0.01$ ; RBAR = 0.38; Figure 4A). The chronology is statistically reliable from 1875 to 2018 based on the expressed population signal (EPS), which exceeded 0.85. The chronology of *H. courbaril* (1783 to 2018), based on 47 radii from 24 trees (45% of all the sampled trees), and *P. paniculata* (1850 to 2018), based on 40 radii from 14 trees (35% of all the sampled trees), presented a significant mean correlation among the series ( $r = 0.41$ ,  $p < 0.01$ , Figure 4B; and  $r = 0.40$ ,  $p < 0.01$ , Figure 4C, respectively). The RBAR of the chronologies was 0.2 and 0.17 for *H. courbaril* and *P. paniculata*, respectively, which verifies the high variability in growth between individuals of the same species, as is common in tropical studies [82,83]. The EPS values ( $\geq 0.85$ ) indicated a good population representation of the chronology from 1840 to 2018 for *H. courbaril* and from 1910 and 2018 for *P. paniculata*. EPS values close to 0.85 are generally accepted as a good level of common signal fidelity among trees [65].

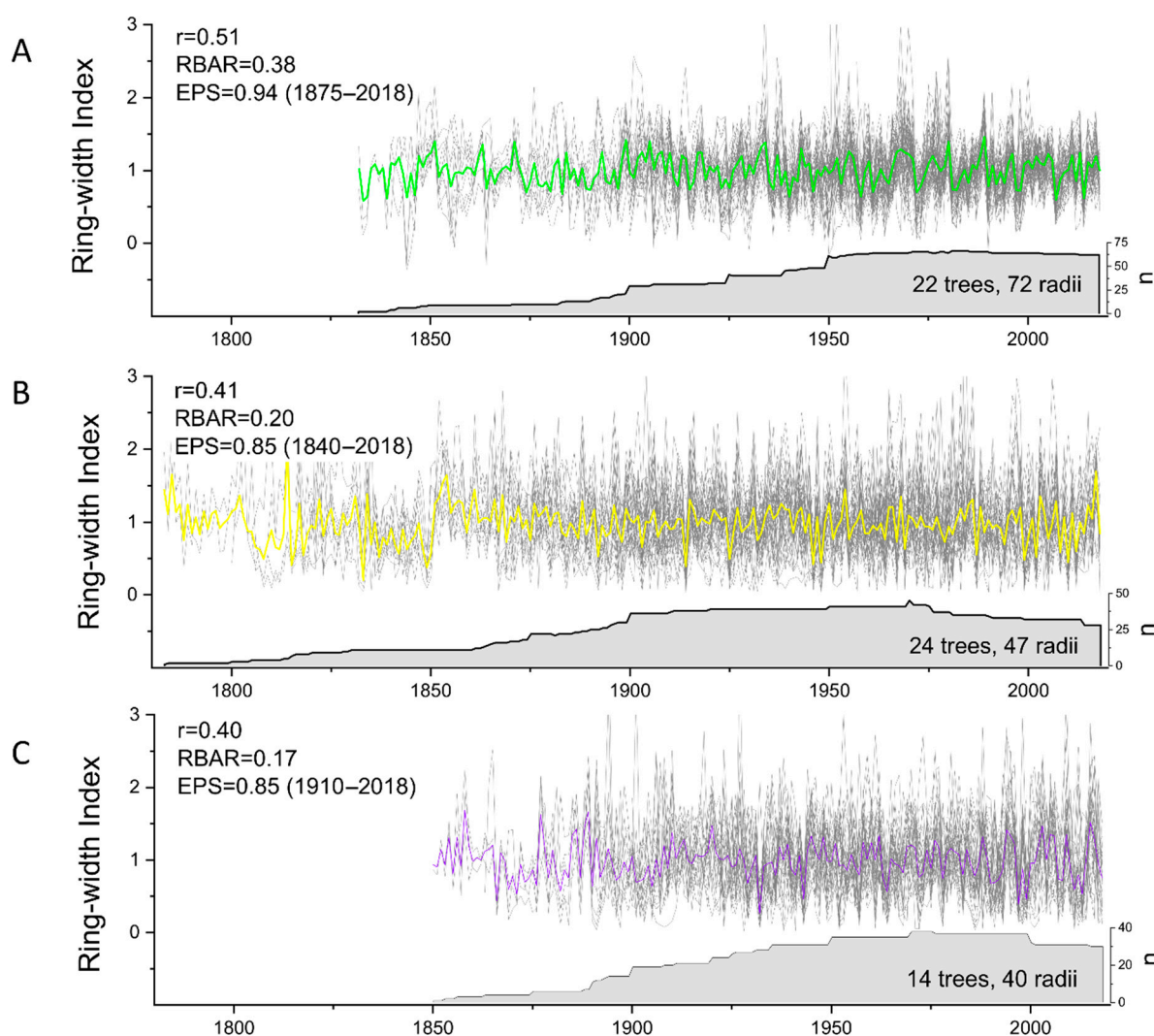


**Figure 4.** All dated, detrended, and standardized radii time series (gray lines) drawn in conjunction with the mean index residual chronology from *Cedrela fissilis* (A), *Hymenaea courbaril* (B), and *Peltogyne paniculata* (C); (green, yellow, and purple, respectively).

EPS values for *H. courbaril* should be taken with caution. Figure 3D and Figure S1 show that *H. courbaril* at JNF shows a small number of wedging rings, where the marginal parenchyma of two to four rings converged on one. The issue was initially detected in one of the radii of the four samples analyzed. The problem was more apparent in rings closer to the pith and in those formed after 1980. Furthermore, the growth rings in these segments of the cross-section showed a low degree of synchronized variation (complacent rings, cf. [84]), hampering the cross-dating between trees and even between radii of the same tree. This may have increased the probability of ring misidentification for this species (see Section 3.3 below), despite showing apparently acceptable dating statistics, as have been observed in other tropical tree species [21,25].

### 3.3. Radiocarbon Analysis

$\alpha$ -Cellulose chemical processing to produce homogenized fibre extracts from wood series and wood reference materials to undergo  $^{14}\text{C}$  analysis were straightforward and did not take more than 5 days in total, including wood cutting to chips and drying processes. Removal of wood extractives was observed visually during the first acid treatment at  $70^\circ\text{C}/30\text{ min}$  of *P. paniculata* selected tree rings: the sample supernatant turned light pink at the first acid bath. Treatment was repeated to ensure effective removal of unwanted

compounds that were clearly soluble in acid. For the duration of the chemical extraction, no further unusual coloring was observed, from supernatants or solids. The resulting fibrous material appeared white and seemed sufficiently pure for isotopic measurements upon analysis, even though organic solvents (typically used when applying the Jayme-Wise method with a Soxhlet system [66]) were not added to the existing chemical protocol.

Table 1 shows the measured  $F^{14}C$  results associated with the seven calendar years selected for all tree species of JNF as well as results from reference materials. Data reliability was evaluated by checking post-AD 1950 reference materials targets, such as OX-II, ANU, and the chemically processed FIRI-J, against their consensus value limits (Table 1). A subfossil FIRI-H wood, subjected to  $\alpha$ -cellulose extraction, was also in excellent agreement with expected  $^{14}C$  value. The average AVR wood blank processed to  $\alpha$ -cellulose and used to correct tree-ring  $^{14}C$  results was statistically indistinguishable from the combustible POC coal target, and yielded a radiocarbon age equivalent to 53.7 kyrs BP on average.

**Table 1.** JNF tree species and reference materials  $^{14}C$  data.

UCIAMS#	Tree Species/Sample ID	Calendar Date Adjusted	$F^{14}C$	$\pm 1\sigma$	Weighed Mean $F^{14}C$ †	Propagated Error	Standard Error
241053	JAC09C-1957	1957.08	1.0272	0.0014			
241054	JAC09C-1958	1958.08	1.0689	0.0014			
241055	JAC09C-1962	1962.08	1.2068	0.0016			
241056	JAC09C-1963(1)	1963.08	1.2868	0.0017			
241057	JAC09C-1963(2)	1963.08	1.2849	0.0017	1.2858	0.0012	0.0009
241058	JAC09C-1965	1965.08	1.6282	0.0025			
241059	JAC09C-1971	1971.08	1.4957	0.0022			
241060	JAC09C-1972	1972.08	1.4780	0.0020			
241036	JAJ30A-1957	1957.08	0.9818	0.0014			
241037	JAJ30A-1958	1958.08	0.9799	0.0014			
241038	JAJ30A-1962(1)	1962.08	0.9870	0.0017			
241039	JAJ30A-1962(2)	1962.08	0.9889	0.0014	0.9881	0.0011	0.0009
241040	JAJ30A-1963	1963.08	1.0013	0.0014			
241041	JAJ30A-1965	1965.08	1.0634	0.0018			
241042	JAJ30A-1971	1971.08	1.6062	0.0024			
241043	JAJ30A-1972	1972.08	1.5928	0.0023			
241045	JAR26C-1957	1957.08	1.0312	0.0014			
241046	JAR26C-1958	1958.08	1.0605	0.0016			
241047	JAR26C-1962	1962.08	1.1989	0.0017			
241048	JAR26C-1963(1)	1963.08	1.2802	0.0018			
245722	JAR26C-1963(2)	1963.08	1.2816	0.0018	1.2809	0.0013	0.0007
241050	JAR26C-1965	1965.08	1.6574	0.0022			
241051	JAR26C-1971	1971.08	1.5013	0.0020			
241052	JAR26C-1972	1972.08	1.4824	0.0022			
<b>Reference materials (extracted to <math>\alpha</math>-cellulose)</b>							
UCIAMS#	Sample ID	Expected $F^{14}C$ values §	$F^{14}C$	$\pm 1\sigma$	Weighed Mean $F^{14}C$ †	Propagated Error	Standard Error
241079	FIRI-J barley	~1.107	1.1019	0.0015			
241080			1.1073	0.0015	1.1046	0.0011	0.0027
241083	FIRI-H fossil wood	~0.757	0.7576	0.0011			
241081	AVR $^{14}C$ -free wood	>55 kyrs	0.0013 *	0.0000			
241082			0.0012 *	0.0000	0.0012	0.0000	0.0000

Table 1. Cont.

Reference materials (combusted)							
245696	OX2 (oxalic-acid)	~1.340	1.3407	0.0019			
245705			1.3374	0.0019	1.3390	0.0013	0.0016
245706	ANU sucrose	~1.502	1.5023	0.0022			
241044			1.5037	0.0023	1.5030	0.0016	0.0007
241034	POC Coal	>55 kyrs	0.0013 *	0.0000			

Note: UCIAMS# refers to laboratory code results associated to individual measurements. \* These results correspond to the associated background blank acquired during chemical processing and/or just  $^{14}\text{C}$  graphite target processing. Therefore, they were not background-corrected by any means. † For uncertainty discussions of replicated data, we used the error-weighted mean and the largest between propagated and standard error (see text for details). § Consensus values of reference materials for internal laboratory data quality control can be found in multiple publications (e.g., [68–70] and references therein).

Reproducibility was evaluated based on duplicated measurements of reference materials (combustibles or extracts) as well as JNF duplicates of selected calendar years. Although we produced just three pairs in total from JNF  $\alpha$ -cellulose extracts, their error-weighted mean among duplicates was equal or lower than 0.13%, and better than the individual error (Table 1). As already stated, individual target error includes all systematic propagated errors—i.e., counting statistics, primary and secondary standard measurement accuracy/precision, isotopic fractionation, as well as background corrections (details in [70]). Essentially, reproducibility was at a 0.2% level for all duplicates, except for OX2, which was 0.27%.

Radiocarbon results pertaining to the same calendar years but from coexisting tree species from sites separated by less than 10 km—e.g., *C. fissilis* (JAC09C) and *P. paniculata* (JAR26C)—also yielded similar  $^{14}\text{C}$  signatures (within  $\pm 2\sigma$ ), except for the results concerning the calendar year 1965 (at the highest and greatest noise portion of the bomb-shaped curve). Still, reproducibility was within the 1.4% level—i.e., good to excellent—taking into account that these are two different tree species with lifecycles that are most likely slightly misaligned.

To validate whether the JNF tree species are annual in nature, and to verify whether the tree species/site chronologies attained for them are robust, we plotted the  $\text{F}^{14}\text{C}$  associated value of each calendar year's individual tree rings alongside the current atmospheric post-AD 1950  $^{14}\text{C}$  calibration curves (see Figure 5). Since air masses transporting  $^{14}\text{C}$  and influencing the JNF site are presently undefined—i.e., JNF falls within the U-shaped boundary of the TLPB and the western side of the actual boundary itself [44]—we used both SH datasets from the designated atmospheric  $^{14}\text{C}$  zones (SH zone 1–2 and 3), defined in [27], to produce Figure 5. Calendar dates were also adjusted to a small decimal date (i.e.,  $0.08 \pm 0.15$  was added to each calendar year) to better represent the middle of the expected maximum growing season. The annual decimal date was inferred based on the length and amount of the region's precipitation (Figure 1C), and best fitting of calendar dendrochronology dates to bomb curve. The data cover a length of approximately 4 months in total, which started at the preceding calendar year and spilled over to the next year, placing the maximum growth where precipitation was already well established. This type of anchoring and adjustment by calendar dates has been proven to work well for tree species and settings across the Pantropical region (e.g., [11,24]).

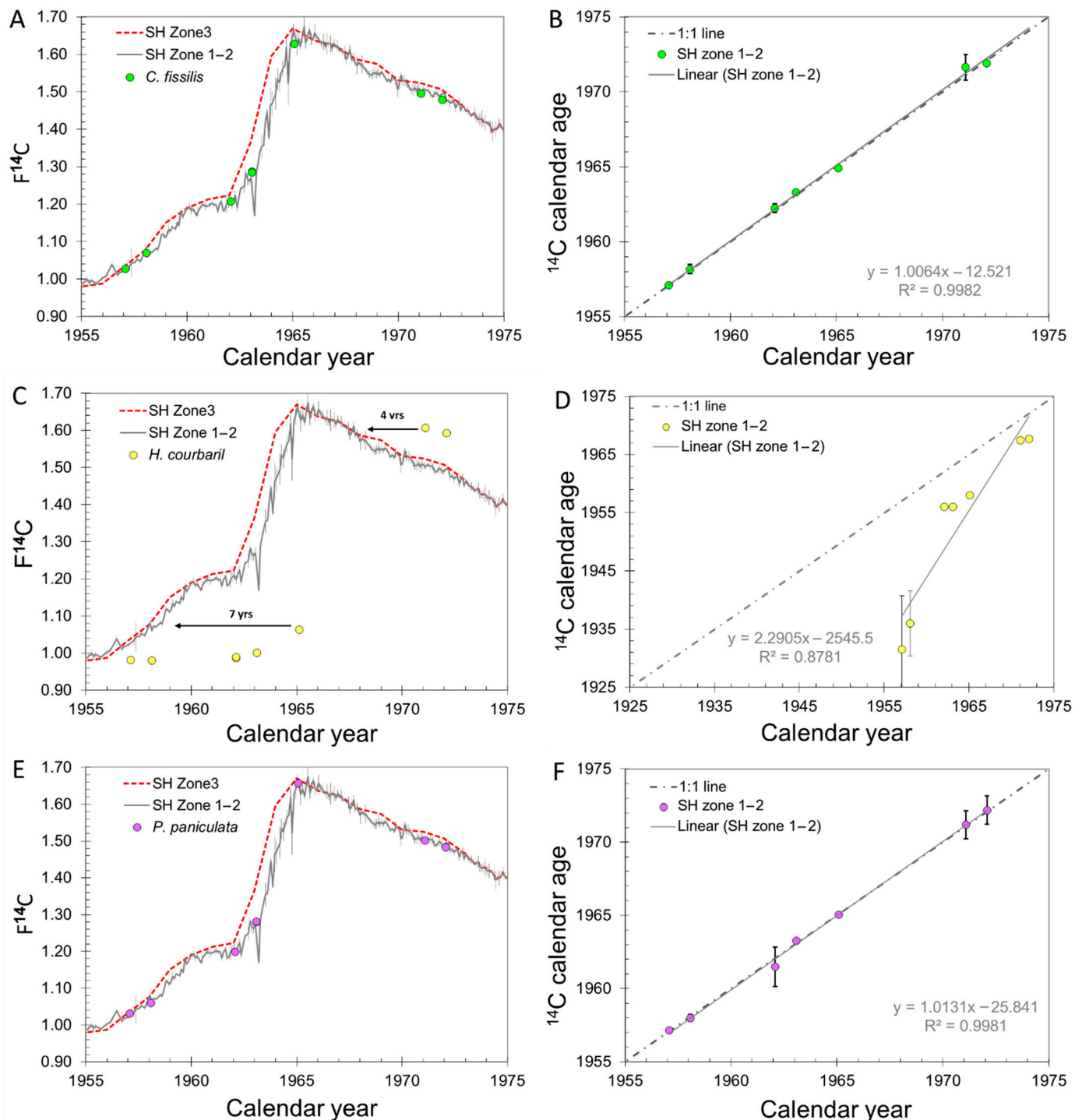


**Figure 5.** Evaluation of annual periodicity was determined by plotting  $F^{14}C$  from 7 tree-rings of selected calendar years against  $^{14}C$  records reported in [27] (left panels), and comparisons of dendrochronological dates and calibrated  $^{14}C$  derived dates (right panels) for *Hymenaea courbaril* (A,B), and *Peltogyne paniculata* (C,D), and *Cedrela fissilis* (E,F). In panels (A,C,E), discrete radiocarbon results were plotted separately. Reproducibility is so tight that  $^{14}C$  results on duplicates ( $n = 2$ ) overlap, and are within uncertainties ( $\pm 1\sigma$ ; Table 1). In panels (B,D,F), curve construction was produced from the average calibrated  $^{14}C$  age obtained using CaliBomb software and SH zone 1–2 dataset. Uncertainties were calculated according to the range of the age interval. Correlation coefficient is shown for each tree species best-fit linear regression, as well as 1:1 dashed line.

In Figure 5 we also plot  $^{14}C$  ages calibrated using CaliBomb (<http://calib.org/CALIBomb/>, accessed 6 April 2021) based on the  $F^{14}C$  values attained from tree ring data versus dendrochronology calendar dates. This is a precise way to visualize the same data, which

clearly predicts whether the annual calendar dates were assigned correctly. It also establishes what SH  $^{14}\text{C}$  zonal region these tree species/site belong to: i.e., whether or not air masses reaching sites originate mostly from outside the TLPB boundary U-shaped area (e.g., SH zone 1–2). Note that here we already eliminated all calibrated  $^{14}\text{C}$  ages' ambiguities produced by CaliBomb, as the sequence of calendar ages expected was already known at a decimal level (according to rainfall season across the region; Figure 1C). The comparative analysis outlined above attested to each chronology's robustness with respect to tree species' annual growth patterns.

Optimal matches between slightly adjusted dendrochronological dates (Table 1) and atmospheric post-AD 1950  $^{14}\text{C}$  calibration curves were found for *C. fissilis* (JAC09C) and *P. paniculata* (JAR26C) (Figure 5A,E, respectively). Moreover, the remarkable agreement of discrete calibrated  $^{14}\text{C}$  ages versus dendrochronology ages indicated that these tree species were exposed to  $^{14}\text{C}$  air-masses mostly from SH zones 1–2 (Figure 5B,F; dashed line = 1:1 match, solid line = best-fit linear regression,  $R^2 \approx 1$ ). The present finding is significant. At first glance, the current compiled data of global atmospheric  $^{14}\text{C}$ , based mostly on latitudinal differences, place JNF within SH zone 3 [27]. Yet, the boundaries between SH zones 1–2 and zone 3 that are associated with the TLPB over South America are still poorly defined [11], and bear a huge uncertainty [44]. While highly speculative, as just 7 tree-ring calendar years from these tree species have been measured so far, it is possible that we have found the right region across the Amazon Basin for studying TLPB space-time variability where the positive atmospheric  $^{14}\text{C}$  gradient is disrupted, forming two distinct zones. A full sequence of tree ring  $^{14}\text{C}$  measurements of one or both of these tree species would be required to better elucidate the atmospheric circulation pattern and the carbon reservoir provenances affecting this region [44,85].

With regard to the  $^{14}\text{C}$  results of the *H. courbaril* (JA30A), which have been shown to be annual at Panama [28], we found an erratic sequence of wood ages at JNF (Table 1, Figure 5C,D). According to the yielded  $\text{F}^{14}\text{C}$  results attained from the dendrochronology dates provided, at least seven calendar years were not detected during ring counting due to the presence of extra wedged rings undetected during ring demarcation. This is the most acceptable explanation for the offset detected in the  $^{14}\text{C}$  measurements. A second explanation would be random absence of rings. But this would imply that cambial dormancy for this tree species at this location (about 20 km south of the other two tree species in this study) is linked to something other than precipitation, resulting in an interesting challenge to be elucidated. Nonetheless, this outcome makes this chronology unfit for further long-term studies, as some ring boundaries remained indistinct (Figure S1) even though a couple of techniques were used to determine the cambial markings (Figure 3). Another worrisome aspect of our  $^{14}\text{C}$  findings here is related to the significant mean correlation values associated with *H. courbaril* chronology (Figure 4B). Alone they would probably be accepted as sufficient proof for chronology robustness. But after our independent evaluation—i.e., post-AD 1950  $^{14}\text{C}$  validation—an EPS value of 0.85 and associated parameters did not provide a clear-cut test for verifying annual ring formation in tropical trees (at least not for this tropical tree species/site).

#### 4. Implications for Tropical Dendrochronology and Atmospheric $^{14}\text{C}$ New Records

Cross-dating provides absolute correspondence dates of specific rings within different specimens and, ultimately, an absolute date for each ring by matching the ring width patterns among specimens at a given site [86]. This is the backbone of the dendrochronology technique. These techniques were applied to *C. fissilis*, *H. courbaril*, and *P. paniculata* at the JNF (Figure 1), a small protected area surrounded by a degraded forest due to decades of land cover change, in order to produce tree-ring width chronologies. Accuracy and reliability of dating were controlled by observation (e.g., Skeleton plot) and statistical correlation assessments (e.g., COFECHA) and were found to be satisfactory for all chronologies produced in this study. However, once tree ring chronologies were carefully evaluated by post-AD 1950  $^{14}\text{C}$  measurements of selected tree rings (Table 1, Figure 5), an offset was

detected on *H. courbaril* chronology, implying that several rings were missed due to their indistinguishable anatomical features (Figure S1). This has important implications for tropical dendrochronology, as it illustrates again how identifying the growth-ring boundaries in some tropical tree species/sites is very problematic and can be somewhat unpredictable. In contrast to temperate climates (with well-demarcated wet and dry seasons), the subtle changes of tropical climates, and consequently the poor demarcation of ring boundaries, call for validation of the annual periodicity of the tree rings using independent methods differing from those found in the extra-tropics. Therefore, we postulate that high-precision validation by  $^{14}\text{C}$  should be adopted when studying tree-ring chronologies in the tropics (see [11,20,22,24], for example).

As already mentioned, the calendar years selected for corroborating the dendrochronology dates are from a period where the differences in atmospheric  $^{14}\text{C}$  between consecutive calendar years are the highest. A perfect agreement between dendrochronological dates' assigned and expected  $^{14}\text{C}$  values would imply that in addition to successfully achieving the primary goal of annual validation, tree species candidates can be used as paleo proxies, and material (tree rings) also can be selected to extend observational atmospheric  $^{14}\text{C}$  records [11]. We also postulate that either *C. fissilis* (JAC09C) and/or *P. paniculata* (JAR26C) are excellent candidates to represent the southwestern side of the U shape associated with the TLPB [44], and should be considered in further studies for the long-term atmospheric  $^{14}\text{C}$  global map [11].

## 5. Conclusions

In this study, tree ring width chronologies of *C. fissilis* (1875 to 2018), *H. courbaril* (1840 to 2018), and *P. paniculata* (1910 to 2018) were developed by standard dendrochronological techniques in the southwestern Brazilian Amazonia Basin. This also was the first attempt to build a tree-ring width chronology using *P. paniculata* tree species. Although chronology statistical parameters are generally commonly acceptable to determine chronology fitness among dendrochronologists, these parameters can still miss the mark when dealing with new tree species in the tropics.

Here, we used post-AD 1950  $^{14}\text{C}$  measurements of selected tree rings and determined that while the *H. courbaril* tree species from JNF is unsuited to moving forward within dendrochronology applications due to indistinguishable features (missed during cross-dating), *C. fissilis* and *P. paniculata* tree species are annual in nature, and their chronologies align perfectly with expected values. This independent validation was performed by high-precision determinations at KCCAMS/UCI on  $\alpha$ -cellulose fibres, using a substantial number of duplicates of reference materials and tree rings, giving absolute confidence in the final results and assigned dendrochronological dates. In this sense, *C. fissilis* and *P. paniculata* growth rings can be used as a powerful proxy indicator of climate variability. Moreover, due to the sampling site's strategic location in relation to the TLPB, the dendrochronologically-dated tree rings of *C. fissilis* and/or *P. paniculata* also can be used to enhance the limited amount of observational data for the Southern Hemisphere atmospheric  $^{14}\text{C}$  at lower latitudes.

**Supplementary Materials:** The following are available online at <https://www.mdpi.com/article/10.3390/f12091177/s1>. Figure S1. Examples of doubtful growth rings (GR) in *Hymenaea courbaril*; marginal parenchyma of two to four rings converge into one.

**Author Contributions:** Conceptualization, Radiocarbon Methodology, Supervision, Investigation, Formal analysis and interpretation, Funding acquisition, Writing—original draft, visualization, data curation, validation, literature synthesis and discussion, G.M.S.; Tree-ring Methodology, Investigation, Writing—original draft, visualization, literature synthesis and discussion, D.R.O.R., N.d.O.B. and G.A.-P.; Tree-ring Methodology, Supervision, Writing—original draft, visualization, and discussion, A.C.B.; Tree ring Methodology, Supervision, Resources, Funding acquisition, Writing—review & editing, F.A.R. and M.T.-F. All authors have read and agreed to the published version of the manuscript.

**Funding:** This research was supported by a U.S. National Science Foundation grant to GMS (NSF AGS-1903690). This contribution is part of the PhD thesis of DROR at the ESALQ-USP, which was supported by a fellowship from the Fundação de Amparo à Pesquisa do Estado do São Paulo (FAPESP; grant # 2018/22914-8). NOB was supported from FAPESP (grant # 2019/26350-4). GAP was supported by CAPES (grant # 88887.199858/2018-00) through the National Academic Cooperation Program in the Amazon. This study was also partially funded by Wood Anatomy and Tree-Ring Laboratory (LAIM) (FAPESP; grant # 2009/53951-7), Laboratory of Dedrochronology at UFLA (FAPEMIG), and PIRE-project (FAPESP; grant # 2017/50085-3).

**Data Availability Statement:** Data pertaining to this research work appears in Table 1. Supporting 14C records used in comparisons are properly cited in text and reference list, and appear in Supplementary Materials of these works.

**Acknowledgments:** GMS appreciated the help of Xiaomei Xu and Claudia Czimczik during data analysis and KCCAMS/UCI facility support. The authors thank (SISBIO) ICMBio for the collection license #66094. Additional thanks to the logging firms AMATA and MADEFLONA for their assistance in the field.

**Conflicts of Interest:** The authors declare no conflict of interest. Also, the funders had no role in the design of the study; in the collection, analyses, or interpretation of data; in the writing of the manuscript, or in the decision to publish the results.

## References

- Schweingruber, F.H. *Tree Rings: Basics and Applications of Dendrochronology*; Springer: Dordrecht, The Netherlands, 2012; ISBN 978-94-009-1273-1.
- Stahle, D.W.; Cook, E.R.; Burnette, D.J.; Villanueva, J.; Cerano, J.; Burns, J.N.; Griffin, D.; Cook, B.I.; Acuña, R.; Torbenson, M.C.; et al. The Mexican Drought Atlas: Tree-ring reconstructions of the soil moisture balance during the late pre-Hispanic, colonial, and modern eras. *Quat. Sci. Rev.* **2016**, *149*, 34–60. [[CrossRef](#)]
- Gholami, V.; Torkaman, J.; Dalir, P. Simulation of precipitation time series using tree-rings, earlywood vessel features, and artificial neural network. *Theor. Appl. Clim.* **2018**, *137*, 1939–1948. [[CrossRef](#)]
- Matskovsky, V.; Venegas-González, A.; Garreaud, R.; Roig, F.A.; Gutiérrez, A.G.; Muñoz, A.A.; Le Quesne, C.; Klock, K.; Canales, C. Tree growth decline as a response to projected climate change in the 21st century in Mediterranean mountain forests of Chile. *Glob. Planet. Chang.* **2021**, *198*, 103406. [[CrossRef](#)]
- Pompa-García, M.; Camarero, J.J. *Latin American Dendroecology: Combining Tree-Ring Sciences and Ecology in a Megadiverse Territory*; Springer International Publishing: Cham, Switzerland, 2020. [[CrossRef](#)]
- Schöngart, J.; Bräuning, A.; Barbosa, A.C.M.C.; Lisi, C.S.; De Oliveira, J.M. Dendroecological Studies in the Neotropics: History, Status and Future Challenges. In *Dendroecology*; Amoroso, M., Daniels, L., Baker, P., Camarero, J., Eds.; Ecological Studies (Analysis and Synthesis); Springer: Cham, Switzerland, 2017; Volume 231. [[CrossRef](#)]
- Nath, C.D.; Munoz, F.; Péliissier, R.; Burslem, D.; Muthusankar, G. Growth rings in tropical trees: Role of functional traits, environment, and phylogeny. *Trees* **2016**, *30*, 2153–2175. [[CrossRef](#)]
- Silva, M.D.S.; Funch, L.S.; Da Silva, L.B. The growth ring concept: Seeking a broader and unambiguous approach covering tropical species. *Biol. Rev.* **2019**, *94*, 1161–1178. [[CrossRef](#)] [[PubMed](#)]
- Worbes, M. One hundred years of tree-ring research in the tropics—A brief history and an outlook to future challenges. *Dendrochronologia* **2002**, *20*, 217–231. [[CrossRef](#)]
- Santos, G.; Linares, R.; Lisi, C.; Filho, M.T. Annual growth rings in a sample of Paraná pine (*Araucaria angustifolia*): Toward improving the 14C calibration curve for the Southern Hemisphere. *Quat. Geochronol.* **2015**, *25*, 96–103. [[CrossRef](#)]
- Santos, G.M.; Granato-Souza, D.; Barbosa, A.C.; Oelkers, R.; Andreu-Hayles, L. Radiocarbon analysis confirms annual periodicity in *Cedrela odorata* tree rings from the equatorial Amazon. *Quat. Geochronol.* **2020**, *58*, 101079. [[CrossRef](#)]
- Reimer, P.J.; Austin, W.E.N.; Bard, E.; Bayliss, A.; Blackwell, P.G.; Bronk Ramsey, C.; Butzin, M.; Cheng, H.; Edwards, R.L.; Friedrich, M.; et al. The IntCal20 Northern Hemisphere Radiocarbon Age Calibration Curve (0–55 cal kBP). *Radiocarbon* **2020**, *62*, 725–757. [[CrossRef](#)]
- Hogg, A.G.; Heaton, T.J.; Hua, Q.; Palmer, J.G.; Turney, C.S.; Southon, J.; Bayliss, A.; Blackwell, P.G.; Boswijk, G.; Ramsey, C.B.; et al. SHCal20 Southern Hemisphere Calibration, 0–55,000 Years cal BP. *Radiocarbon* **2020**, *62*, 759–778. [[CrossRef](#)]
- Levin, I.; Hesshaimer, V. Radiocarbon—A Unique Tracer of Global Carbon Cycle Dynamics. *Radiocarbon* **2000**, *42*, 69–80. [[CrossRef](#)]
- Santos, G.M. Beyond archaeology: 14C-AMS and the global carbon cycle. In *AIP Conference Proceedings*; American Institute of Physics: College Park, MD, USA, 2012; Volume 1423, pp. 311–318. [[CrossRef](#)]
- Graven, H.D. Impact of fossil fuel emissions on atmospheric radiocarbon and various applications of radiocarbon over this century. *Proc. Natl. Acad. Sci. USA* **2015**, *112*, 9542–9545. [[CrossRef](#)] [[PubMed](#)]
- National Centers for Environmental Information (NOAA). Paleoclimatology Data Map—NCEI-Map Application. Available online: <https://gis.ncdc.noaa.gov/maps/ncei/paleo?layers=0000000000000001>. (accessed on 20 April 2021).



18. Babst, F.; Poulter, B.; Bodesheim, P.; Mahecha, M.; Frank, D. Improved tree-ring archives will support earth-system science. *Nat. Ecol. Evol.* **2017**, *1*, 8. [[CrossRef](#)]
19. Rozendaal, D.M.A.; Zuidema, P. Dendroecology in the tropics: A review. *Trees* **2010**, *25*, 3–16. [[CrossRef](#)]
20. Wils, T.H.; Robertson, I.; Eshetu, Z.; Sass-Klaassen, U.G.; Koprowski, M. Periodicity of growth rings in *Juniperus procera* from Ethiopia inferred from crossdating and radiocarbon dating. *Dendrochronologia* **2009**, *27*, 45–58. [[CrossRef](#)]
21. Herrera-Ramirez, D.; Andreu-Hayles, L.; Del Valle, J.I.; Santos, G.; Gonzalez, P.L.M. Nonannual tree rings in a climate-sensitive *Prioria copaifer* chronology in the Atrato River, Colombia. *Ecol. Evol.* **2017**, *7*, 6334–6345. [[CrossRef](#)] [[PubMed](#)]
22. Haines, H.A.; Olley, J.M.; English, N.; Hua, Q. Anomalous ring identification in two Australian subtropical *Araucariaceae* species permits annual ring dating and growth-climate relationship development. *Dendrochronologia* **2018**, *49*, 16–28. [[CrossRef](#)]
23. Vetter, R.E.; Botosso, P.C. Remarks on Age and Growth Rate Determination of Amazonian Trees. *IAWA J.* **1989**, *10*, 133–145. [[CrossRef](#)]
24. Baker, J.C.A.; Santos, G.M.; Gloor, M.; Brienen, R.J.W. Does *Cedrela* always form annual rings? Testing ring periodicity across South America using radiocarbon dating. *Trees* **2017**, *31*, 1999–2009. [[CrossRef](#)] [[PubMed](#)]
25. Soliz-Gamboa, C.C.; Rozendaal, D.M.A.; Ceccantini, G.; Angyalossy, V.; Van Der Borg, K.; Zuidema, P.A. Evaluating the annual nature of juvenile rings in Bolivian tropical rainforest trees. *Trees* **2010**, *25*, 17–27. [[CrossRef](#)]
26. Enting, I.G. *Nuclear Weapons Data for Use in Carbon Cycle Modelling*; C.S.I.R.O: Melbourne, Australia, 1982; ISBN 0 643 03460 9.
27. Hua, Q.; Barbetti, M.; Rakowski, A. Atmospheric Radiocarbon for the Period 1950–2010. *Radiocarbon* **2013**, *55*, 2059–2072. [[CrossRef](#)]
28. Westbrook, J.A.; Guilderson, T.P.; Colinvaux, P.A. Annual Growth Rings in a Sample of *Hymenaea Courbaril*. *IAWA J.* **2006**, *27*, 193–197. [[CrossRef](#)]
29. Hadad, M.A.; Santos, G.M.; Juñent, F.A.R.; Grainger, C.S. Annual nature of the growth rings of *Araucaria araucana* confirmed by radiocarbon analysis. *Quat. Geochronol.* **2015**, *30*, 42–47. [[CrossRef](#)]
30. Andreu-Hayles, L.; Santos, G.; Herrera-Ramírez, D.; Martín-Fernández, J.; Ruiz-Carrascal, D.; Boza-Espinoza, T.; Fuentes, A.; Jorgensen, P. Matching Dendrochronological Dates with the Southern Hemisphere <sup>14</sup>C Bomb Curve to Confirm Annual Tree Rings in *Pseudolmedia Rigida* from Bolivia. *Radiocarbon* **2015**, *57*, 1–13. [[CrossRef](#)]
31. Biondi, F.; Fessenden, J.E. Radiocarbon Analysis of *Pinus Lagunae* Tree Rings: Implications for Tropical Dendrochronology. *Radiocarbon* **1999**, *41*, 241–249. [[CrossRef](#)]
32. Godoy-Veiga, M.; Cintra, B.B.L.; Stríkis, N.M.; Cruz, F.W.; Grohmann, C.H.; Santos, M.S.; Regev, L.; Boaretto, E.; Ceccantini, G.; Locosselli, G.M. The value of climate responses of individual trees to detect areas of climate-change refugia, a tree-ring study in the Brazilian seasonally dry tropical forests. *For. Ecol. Manag.* **2021**, *488*, 118971. [[CrossRef](#)]
33. Barbosa, A.C.M.; Pereira, G.A.; Granato-Souza, D.; Santos, R.M.; Fontes, M.A.L. Tree rings and growth trajectories of tree species from seasonally dry tropical forest. *Aust. J. Bot.* **2018**, *66*, 414. [[CrossRef](#)]
34. Pereira, G.D.A.; Barbosa, A.C.M.C.; Torbenson, M.; Stahle, D.W.; Granato-Souza, D.; Dos Santos, R.M.; Barbosa, J.P.D. The Climate Response of *Cedrela Fissilis* Annual Ring Width in the Rio São Francisco Basin, Brazil. *Tree-Ring Res.* **2018**, *74*, 162–171. [[CrossRef](#)]
35. Hammerschlag, I.; Macario, K.D.; Barbosa, A.C.; Pereira, G.D.A.; Farrapo, C.L.; Cruz, F. Annually Verified Growth of *Cedrela Fissilis* from Central Brazil. *Radiocarbon* **2019**, *61*, 927–937. [[CrossRef](#)]
36. Locosselli, G.M.; Buckeridge, M.; Moreira, M.Z.; Ceccantini, G. A multi-proxy dendroecological analysis of two tropical species (*Hymenaea* spp., *Leguminosae*) growing in a vegetation mosaic. *Trees* **2012**, *27*, 25–36. [[CrossRef](#)]
37. Locosselli, G.M.; Schongart, J.; Ceccantini, G. Climate/growth relations and teleconnections for a *Hymenaea courbaril* (*Leguminosae*) population inhabiting the dry forest on karst. *Trees* **2016**, *30*, 1127–1136. [[CrossRef](#)]
38. Brienen, R.J.W.; Zuidema, P. Relating tree growth to rainfall in Bolivian rain forests: A test for six species using tree ring analysis. *Oecologia* **2005**, *146*, 1–12. [[CrossRef](#)] [[PubMed](#)]
39. Pedlowski, M.A.; Dale, V.H.; Matricardi, E.A.; Filho, E.P.D.S. Patterns and impacts of deforestation in Rondônia, Brazil. *Landsc. Urban Plan.* **1997**, *38*, 149–157. [[CrossRef](#)]
40. Germer, S.; Neill, C.; Krusche, A.; Neto, S.C.G.; Elsenbeer, H. Seasonal and within-event dynamics of rainfall and throughfall chemistry in an open tropical rainforest in Rondônia, Brazil. *Biogeochemistry* **2007**, *86*, 155–174. [[CrossRef](#)]
41. Khanna, J.; Medvigy, D.; Fueglistaler, S.; Walko, R. Regional dry-season climate changes due to three decades of Amazonian deforestation. *Nat. Clim. Chang.* **2017**, *7*, 200–204. [[CrossRef](#)]
42. Leite-Filho, A.T.; Soares-Filho, B.S.; Davis, J.L.; Abrahão, G.M.; Börner, J. Deforestation reduces rainfall and agricultural revenues in the Brazilian Amazon. *Nat. Commun.* **2021**, *12*, 1–7. [[CrossRef](#)] [[PubMed](#)]
43. De Sales, F.; Santiago, T.; Biggs, T.W.; Mullan, K.; Sills, E.O.; Monteverde, C. Impacts of Protected Area Deforestation on Dry-Season Regional Climate in the Brazilian Amazon. *J. Geophys. Res. Atmos.* **2020**, *125*. [[CrossRef](#)]
44. Ancapichún, S.; De Pol-Holz, R.; Christie, D.A.; Santos, G.M.; Collado-Fabbri, S.; Garreaud, R.; Lambert, F.; Orfanoz-Cheuquela, A.; Rojas, M.; Southon, J.; et al. Radiocarbon bomb-peak signal in tree-rings from the tropical Andes register low latitude atmospheric dynamics in the Southern Hemisphere. *Sci. Total Environ.* **2021**, *774*, 145126. [[CrossRef](#)]
45. Marengo, J.A.; Liebmann, B.; Grimm, A.M.; Misra, V.; Silva Dias, P.L.; Cavalcanti, I.F.A.; Carvalho, L.M.V.; Berbery, E.H.; Ambrizzi, T.; Vera, C.S.; et al. Recent developments on the South American monsoon system. *Int. J. Climatol.* **2012**, *32*, 1–21. [[CrossRef](#)]
46. Marengo, J.A. Long-term trends and cycles in the hydrometeorology of the Amazon basin since the late 1920s. *Hydrol. Process.* **2009**, *23*, 3236–3244. [[CrossRef](#)]

47. Granato-Souza, D.; Stahle, D.W.; Barbosa, A.; Feng, S.; Torbenson, M.; Pereira, G.D.A.; Schongart, J.; Barbosa, J.P.; Griffin, D. Tree rings and rainfall in the equatorial Amazon. *Clim. Dyn.* **2019**, *52*, 1857–1869. [CrossRef]
48. Ministério do Meio Ambiente. Diagnostico. In *Plano de Manejo da Floresta Nacional do Jamari*; Ministério do Meio Ambiente, Instituto Brasileiro de Meio Ambiente e dos Recursos Naturais Renováveis: Brasília, Brazil, 2005; Volume 1. Available online: [https://www.icmbio.gov.br/portal/images/stories/docs-planos-de-manejo/flona\\_jamari\\_pm\\_diagnostico.pdf](https://www.icmbio.gov.br/portal/images/stories/docs-planos-de-manejo/flona_jamari_pm_diagnostico.pdf) (accessed on 18 April 2021).
49. IBGE. Cidades e Estados. Available online: <https://cidades.ibge.gov.br/> (accessed on 18 April 2021).
50. Instituto Brasileiro de Geografia e Estatística. *Manual Técnico da Vegetação Brasileira*; Instituto Brasileiro de Geografia e Estatística: Rio de Janeiro, Brazil, 2012; ISBN 9788524042720.
51. Bastos, A.; Manisesi, V.; Passos, E.; Gomes, F.; Uchôa, L. Physical Environment Aspects as Subsidy to Occupation in Southwest Amazon Conservation Units—A Case Study Relating the Jamari National Forest and its Surrounding Areas. *Int. J. Sustain. Land Use Urban Plan.* **2015**, *2*, 9–22. [CrossRef]
52. Perigolo, N.A. Caracterização dos Tipos Vegetacionais do Médio Rio Madeira, Rondônia. Master's Thesis, Universidade de Brasília, Brasília, Brazil, 2014. Available online: <https://repositorio.unb.br/handle/10482/17564>. (accessed on 19 April 2021).
53. EMBRAPA. *Sistema Brasileiro de Classificação de Solos*; Embrapa Solos (Empresa Brasileira de Pesquisa Agropecuária): Brasília, Brazil, 2006; ISBN 978-85-7035-198-2.
54. Lobão, M.S. Dendrocronologia, Fenologia, Atividade Cambial e Qualidade do Lenho de Árvores de *Cedrela odorata* L., *Cedrela fissilis* Vell. e *Schizolobium parahyba* var. *amazonicum* Hub. ex Ducke, no estado do Acre. Brasil. Ph.D. Thesis, University of São Paulo, São Paulo, Brazil, 2011. [CrossRef]
55. Souza, I.M.; Funch, L.S. Synchronization of leafing and reproductive phenological events in *Hymenaea* L. species (Leguminosae, Caesalpinioideae): The role of photoperiod as the trigger. *Braz. J. Bot.* **2017**, *40*, 125–136. [CrossRef]
56. Alencar, J.D.C.; De Almeida, R.A.; Fernandes, N.P. Fenologia de espécies florestais em floresta tropical úmida de terra firme na Amazônia Central. *Acta Amaz.* **1979**, *9*, 163–199. [CrossRef]
57. Stahle, D.W. Useful Strategies for the Development of Tropical Tree-Ring Chronologies. *IAWA J.* **1999**, *20*, 249–253. [CrossRef]
58. Grogan, J.; Schulze, M. The Impact of Annual and Seasonal Rainfall Patterns on Growth and Phenology of Emergent Tree Species in Southeastern Amazonia, Brazil. *Biotropica* **2011**, *44*, 331–340. [CrossRef]
59. Tomazello, M.; Brazolin, S.; Chagas, M.P.; Oliveira, J.T.S.; Ballarin, A.W.; Benjamin, C.A. Application of X-ray technique in nondestructive evaluation of eucalypt wood. *Maderas. Cienc. Tecnol.* **2008**, *10*, 139–149. [CrossRef]
60. Cybis Electronic. CDendro and CooRecorder V7.7. Available online: [www.cybis.se](http://www.cybis.se). (accessed on 22 April 2021).
61. Holmes, R.L. Computer-assisted quality control in tree-ring dating and measurement. *Tree Ring Bull.* **1983**, *43*, 69–78. Available online: <http://hdl.handle.net/10150/261223>. (accessed on 20 April 2021).
62. Cook, E.R. *A Time Series Approach to Tree-Ring Standardisation*; University of Arizona: Tucson, AZ, USA, 1985.
63. Cook, E.; Krusic, P. *Program ARSTAN: A Tree-Ring Standardization Program Based on Detrending and Autoregressive Time Series Modeling, with Interactive Graphics*; Lamont Doherty Earth Observatory, Tree-Ring Laboratory: Palisades, NY, USA, 2005.
64. Cook, E.R.; Pederson, N. *Uncertainty, Emergence, and Statistics in Dendrochronology*; Springer: Dordrecht, The Netherlands, 2011; pp. 77–112. [CrossRef]
65. Wigley, T.M.L.; Briffa, K.R.; Jones, P.D. On the Average Value of Correlated Time Series, with Applications in Dendroclimatology and Hydrometeorology. *J. Clim. Appl. Meteorol.* **1984**, *23*, 201–213. [CrossRef]
66. Southon, J.R.; Magana, A.L. A Comparison of Cellulose Extraction and ABA Pretreatment Methods for AMS 14C Dating of Ancient Wood. *Radiocarbon* **2010**, *52*, 1371–1379. [CrossRef]
67. Santos, G.M.; Ormsby, K. Behavioral Variability in ABA Chemical Pretreatment Close to the 14C Age Limit. *Radiocarbon* **2013**, *55*, 534–544. [CrossRef]
68. Santos, G.M.; Xu, X. Bag of Tricks: A Set of Techniques and other Resources to Help 14C Laboratory Setup, Sample Processing, and Beyond. *Radiocarbon* **2017**, *59*, 785–801. [CrossRef]
69. Beverly, R.K.; Beaumont, W.; Tauz, D.; Ormsby, K.M.; Von Reden, K.F.; Santos, G.; Southon, J.R. The Keck Carbon Cycle AMS Laboratory, University of California, Irvine: Status Report. *Radiocarbon* **2010**, *52*, 301–309. [CrossRef]
70. Santos, G.M.; Moore, R.B.; Southon, J.R.; Griffin, S.; Hinger, E.; Zhang, D. AMS 14C Sample Preparation at the KCCAMS/UCI Facility: Status Report and Performance of Small Samples. *Radiocarbon* **2007**, *49*, 255–269. [CrossRef]
71. Reimer, P.J.; Brown, T.; Reimer, R.W. Discussion: Reporting and Calibration of Post-Bomb 14C Data. *Radiocarbon* **2004**, *46*, 1299–1304. [CrossRef]
72. Stuiver, M.; Polach, H.A. Discussion Reporting of 14C Data. *Radiocarbon* **1977**, *19*, 355–363. [CrossRef]
73. IAWA Committee. IAWA List of Microscopic Features for Hardwood Identification. *IAWA Bull.* **1989**, *10*, 219–332. [CrossRef]
74. Moya-Roque, R.; Tomazello-Filho, M. Relationships between anatomical features and intra-ring wood density profiles in *Gmelina arborea* applying X-ray densitometry. *Cerne* **2007**, *13*, 384–392.
75. de Oliveira, B.R.U.; de Figueiredo Latorraca, J.V.; Filho, M.T.; Garcia, R.A.; de Carvalho, A.M. Dendroclimatology correlations of *Eucalyptus grandis* Hill ex Maiden of Rio Claro, RJ state—Brazil. *Ciênc. Florest.* **2011**, *21*, 499–508. [CrossRef]
76. de Andrade, E.S.; dos Santos Carvalho Garcia, S.; Albernaz, A.L.K.M.; Tomazello Filho, M.; Moutinho, V.H.P. Growth ring analysis of *Euxylophora paraensis* through X-ray microdensitometry. *Ciênc. Rural* **2017**, *47*. [CrossRef]

77. De Mil, T.; Tarelkin, Y.; Hahn, S.; Hubau, W.; Deklerck, V.; Debeir, O.; Van Acker, J.; De Cannière, C.; Beeckman, H.; Bulcke, J.V.D. Wood Density Profiles and Their Corresponding Tissue Fractions in Tropical Angiosperm Trees. *Forests* **2018**, *9*, 763. [[CrossRef](#)]
78. Gonçalves, J.Q.; Durgante, F.M.; Wittmann, F.; Piedade, M.T.F.; Rodriguez, D.R.O.; Tomazello-Filho, M.; Parolin, P.; Schöngart, J. Minimum temperature and evapotranspiration in Central Amazonian floodplains limit tree growth of *Nectandra amazonum* (Lauraceae). *Trees* **2021**, *35*, 1–18. [[CrossRef](#)]
79. Tomazello Filho, M.; Botosso, P.C.; Lisi, C.S. Potencialidade da família Meliaceae para dendrocronologia em regiões tropicais e subtropicais. In *Dendrocronología en América Latina*; Universidad Nacional de Cuyo: Mendoza, Argentina, 2000; pp. 381–431.
80. Callado, C.H.; Roig, F.A.; Tomazello-Filho, M.; Barros, C.F. Cambial growth periodicity studies of south american woody species—A review. *IAWA J.* **2013**, *34*, 213–230. [[CrossRef](#)]
81. Tanaka, A. Avaliação de Anéis de Crescimento de Espécies Florestais de Terra-Firme no Município de Novo Aripuanã—AM. Ph.D. Thesis, Instituto Nacional de Pesquisas da Amazônia, Porto Alegre, Brazil, 2005. Available online: <https://repositorio.inpa.gov.br/handle/1/12268>. (accessed on 20 April 2021).
82. Brienen, R.J.W.; Schöngart, J.; Zuidema, P.A. Tree rings in the tropics: Insights into the ecology and climate sensitivity of tropical trees. In *Tropical Tree Physiology*; Goldstein, G., Santiago, L.S., Eds.; Springer International Publishing: Berlin, Germany, 2016; Volume 6, pp. 439–461. [[CrossRef](#)]
83. Camarero, J.J.; Mendivelso, H.A.; Sánchez-Salguero, R. How past and future climate and drought drive radial-growth variability of three tree species in a Bolivian tropical dry forest. In *Latin American Dendroecology*; Pompa-García, M., Camarero, J.J., Eds.; Springer International Publishing: Berlin, Germany, 2020; pp. 141–167. [[CrossRef](#)]
84. Stokes, M.A.; Smiley, T.L. *An Introduction to Tree-Ring Dating*; University of Arizona Press: Tucson, AZ, USA, 1996; ISBN 0816516804.
85. Randerson, J.T.; Enting, I.G.; Fung, I.Y.; Schuur, E.A.G.; Caldeira, K. Seasonal and latitudinal variability of troposphere  $\Delta^{14}\text{CO}_2$ : Post bomb contributions from fossil fuels, oceans, the stratosphere, and the terrestrial biosphere. *Glob. Biogeochem. Cycles* **2002**, *16*, 59–1–59–19. [[CrossRef](#)]
86. Fritts, H.C. *Tree Rings and Climate*; Academic Press: Cambridge, MA, USA, 1976. [[CrossRef](#)]